Applied Catalysis B: Environmental 158–159 (2014) 217–223

Contents lists available at ScienceDirect

Applied Catalysis B: Environmental

journal homepage: www.elsevier.com/locate/apcatb

Photoelectrochemical production of formic acid and methanol from carbon dioxide on metal-decorated CuO/Cu_2O-layered thin films under visible light irradiation

Da Hye Won [a,1], Chang Hyuck Choi [a,1], Jaehoon Chung [a], Seong Ihl Woo [a,b,*]

[a] Department of Chemical and Biomolecular Engineering, Korea Advanced Institute of Science and Technology, Daejeon 305-701, Republic of Korea
[b] Graduate School of EEWS (BK plus), Korea Advanced Institute of Science and Technology, Daejeon 305-701, Republic of Korea

ARTICLE INFO

Article history:
Received 19 February 2014
Received in revised form 9 April 2014
Accepted 13 April 2014
Available online 21 April 2014

Keywords:
CO_2 reduction
Photoelectrochemical
Copper oxide
Transition metal
Performance degradation

ABSTRACT

As a cathode material for fuel generation from CO_2 reduction in a photoelectrochemical system, layered CuO/Cu_2O films were developed and their surfaces were decorated with transition metals (*i.e.* Ag, Au, Cd, Cu, Pb, and Sn). Deposition of the transition metals effectively enhanced CO_2 conversion to fuel in terms of faradaic efficiency. In particular, Pb/CuO/Cu_2O demonstrated outstanding performance among the transition metals: 0.524 μmol/h cm^2 for formic acid and 0.102 μmol/h cm^2 for methanol with 40.45% of total faradaic efficiency at −0.16 V (*vs.* SHE), which was a higher potential than standard redox potentials of formic acid and methanol formation from CO_2. Moreover, electrochemical impedance spectroscopy (EIS) showed that the deposition of the transition metals onto CuO/Cu_2O electrode effectively generated photo-induced electron–hole pairs under visible light irradiation. However, fast performance degradations of the prepared electrodes were observed during the reactions as well as the disappearances of the photocurrents. X-ray photoelectron spectroscopy (XPS) results revealed that the outer CuO layer was readily reduced to Cu_2O/Cu, and this compositional destruction was responsible for the degradation of the photocurrent by prohibiting transfers of the electrons (or holes) to the active sites.

1. Introduction

Carbon dioxide, the main gas product from fossil fuel combustion, is known as one of the primary greenhouse gases. For efficient consumption of CO_2, various studies on the conversion of CO_2 to useful products have been conducted. However, since CO_2 is chemically stable, the conversion of CO_2 requires large external energy such as a gas phase reaction at high temperature [1,2] or an electrochemical reaction at large overpotential [3,4], which produces more CO_2 than the amount of CO_2 used for the conversion (see Supplementary information). Recently, photochemical and photoelectrochemical systems utilizing the photoenergy have been widely studied as a promising approach to overcome the high energy barrier of CO_2 conversion in an energy-and environment-friendly manner. As a photocathode in this system, various types of p-type semiconductors have been developed such as p-GaP [5,6], p-InP [7–9], p-Si [10–12], p-CdTe [13,14], p-CZTS [15] and p-CIS [16]. In order to resolve the problems of low reactivity, selectivity, and faradaic efficiency, however, semiconductors have been modified with several methods such as usage of homogeneous catalysts including pyridine and imidazole with the semiconductor [5,16,17], anchoring a metal complex electrocatalyst such as a Ru complex on the surface of the semiconductor [7–9,15], or decoration of transition metals on the semiconductor surface [10,12].

Cu-based materials (metallic Cu, CuO, and Cu_2O) are abundant resources that show good performances in electrochemical CO_2 reduction systems with affordable preparation methods [4,18–24]. Moreover, copper oxide is a promising material as a photocathode due to its p-type semiconductor properties and suitable band gap that responds to visible light. In a previous study, the Rajeshwar group developed a morphologically modified CuO–Cu_2O hybrid nanoarray that selectively produced methanol from CO_2 with ~95% faradaic efficiency [25,26]. Despite these advantages of the copper oxide, it has not yet been researched extensively as a photocathode. This is probably due to the poor stability of Cu-based materials

* Corresponding author at: Korea Advanced Institute of Science and Technology, Department of Chemical and Biomolecular Engineering, 373-1 Guseong-dong, Yuseong-gu, Daejeon, Republic of Korea. Tel.:+82 42 350 3918; fax: +82 42 350 3910.
E-mail address: siwoo@kaist.ac.kr (S.I. Woo).
[1] These authors have contributed equally.

http://dx.doi.org/10.1016/j.apcatb.2014.04.021
0926-3373/

against severely reducible experimental conditions. For example, a rapid performance degradation of similar materials has been reported in electrochemical systems [22]. Although the electrode deactivation is an important issue in this research area, the origin of the low stability is not yet fully understood.

Herein, layered structure CuO/Cu_2O thin films were simply prepared by oxidation of Cu foil. To improve performance and increase the reaction selectivity, the surfaces of the CuO/Cu_2O films were modified by various transition metal particles. Using a $Me/CuO/Cu_2O$ thin film as a photocathode (Me = Ag, Au, Cd, Cu, Pb, and Sn), photoelectrochemical reduction of CO_2 to liquid fuels was investigated at higher potential than the standard redox potential of the products under visible light irradiation. It has been reported that the selectivity of products in an electrochemical system was highly determined by the type of transition metals used as the electrode material [3]. Furthermore, in a photochemistry system, a junction with metal and a semiconductor improves the efficiency of photoenergy usage [27–29]. Therefore, we anticipated that using a metal to decorate on CuO/Cu_2O would enhance the catalytic activity and control product selectivity according to the type of metals in the photoelectrochemical system. In addition, the degradation phenomenon of the CuO/Cu_2O-based films in the photoelectrochemical reduction of CO_2 was also investigated through the correlation with compositional changes and photocurrent responses in the reactions by using the X-ray photoelectron spectroscopy (XPS) and electrochemical impedance spectroscopy (EIS) studies.

2. Experimental

2.1. Synthesis of $Me/CuO/Cu_2O$

Cu foil (0.25 mm, 99.99%, Sigma-Aldrich) was pretreated with 1.0 M HCl, and then sonicated in ethanol, acetone, and deionized water, sequentially. CuO/Cu_2O layered thin film was synthesized by oxidation of a cleaned Cu substrate at 400 °C under air flow (100 sccm) for 4 h in a tube furnace. Various transition metals, (*i.e.* Ag, Au, Cd, Cu, Sn, and Pb) were deposited onto the CuO/Cu_2O photoelectrode by photo-assisted electrodeposition at −1.0 V (*vs.* SCE) in the 1 M $NaNO_3$ (Sigma-Aldrich) solutions dissolved in 0.02 M of each metal precursor under UV–visible light illumination for 5 s. The selected metal precursors were $AgNO_3$ (Sigma-Aldrich), $HAuCl_4{\cdot}3.6H_2O$ (Kojima Chemicals CO. LTD.), $CdSO_4$ (Sigma-Aldrich), $CuSO_4$ (Sigma-Aldrich), $SnSO_4$ (Sigma-Aldrich), and $Pb(NO_3)_2$ (Sigma-Aldrich).

2.2. Physical characterizations

The physical characteristics of the prepared photocathodes were analyzed using X-ray diffraction (XRD), an ultraviolet–visible near infrared spectrometer (UV–vis-NIR spectrometer), field emission scanning electron microscope (FESEM), energy dispersive X-ray spectrometer (EDS), and XPS. The XRD patterns were obtained by thin film XRD (RIGAKU D/MAX-RC) using the radiation of a Cu $K\alpha$ source at 30 kV and 60 mA. The band gap of CuO/Cu_2O layered thin film was calculated by Kubelka–Munk function based on the results of a UV–vis-NIR spectrometer (V-570 of Jasco). The deposited metals were observed with the FESEM (Hitachi S-4800) equipped with EDS (Horiba) at an acceleration voltage 5.0 kV. The surface compositions of the prepared photocathodes were investigated by XPS (Sigma Probe of Thermo VG Scientific) equipped with a microfocused monochromator X-ray source.

2.3. Photoelectrochemical test

The measurements of photoelectrochemical activity were performed using an electrochemical analyzer of CHI 700D (CH Instruments Inc.). The reactor was a custom-built Teflon reactor with a quartz window, which enables to reference and counter electrodes to be equipped on both sides of the reactor. A saturated calomel electrode (SCE) and carbon rod were used as reference and counter electrodes, respectively. The carbon rod as a counter electrode was used to prevent the re-oxidation of CO_2 reduction products at the counter electrode, such as formic acid and methanol in the batch cell system [5]. The electrolyte was 0.1 M $KHCO_3$ (Sigma-Aldrich) aqueous solution and analytical grade of water (HPLC Certified Solvent, Burdick &Jackson) was used. The light source was a 450 W Xe lamp (Newport, 66921) equipped with a UV cut-off filter (Newport, 59472). The active area of prepared photoelectrode was 1 cm^2.

2.4. Liquid product analysis

Liquid products were analyzed by 800 MHz ^1H 1D liquid NMR (Bruker Avance) at 25 °C. Internal 2,2-dimethyl-2-silapentane-5-sulfonate was used as a chemical shift reference. The standard solution was 2 mM dimethylsulfoxide (DMSO) and 10 mM phenol in D_2O solvent (Cambridge Isotope Laboratories, Inc.). NMR samples were prepared by mixing 476 μL of product-electrolyte and 24 μL of the standard solution. The amounts of products were calculated by comparing integral areas of formic acid and methanol with phenol and DMSO, respectively. The peak positions were calibrated by purchased formic acid (Sigma-Aldrich) and methanol (Sigma-Aldrich) dissolved in 0.1 M $KHCO_3$ aqueous solutions containing the standard solution (Fig. S1). The positions of formic acid and methanol were the same as those reported in previous research [21].

2.5. Gas product analysis

Gas product analyses were performed with 5890 series 2 of Hewlett Packard gas chromatography equipped with a thermal conductivity detector (TCD). A carboxen-1000 column (12390-U, Supelco) was used, and He (99.999% purity) and Ar (99.999% purity) were used as a reference gas. Oven temperature was maintained at 150 °C and 180 °C for He and Ar, respectively. CO_2 (99.99% purity) was continuously purged into the reactor and vented to the sampling loop with 5 sccm of the gas flow velocity. This flow contained the gas products from photoelectrochemical CO_2 reduction. Aliquots were collected every 10 min during the reaction. Before beginning the photoelectrolysis reaction, CO_2 was purged over 45 min and then photoelectrolysis was started after confirming none of the other peaks in gas chromatography responses except CO_2. The calibration curve for CO was obtained by injecting the mixture gases having different CO concentrations in CO_2 balance.

2.6. Band characterization using Mott–Schottky plots

The Mott–Schottky equation is as follows:

$$\frac{1}{C^2} = \frac{2}{\varepsilon\varepsilon_0 e A^2 N_A}\left(V - V_f - \frac{k_B T}{e}\right)$$

where C is the interfacial capacitance, A is the interfacial area, N_A is the number of acceptors, V is the applied voltage, k_B is Boltzmann's constant, T is the absolute temperature, and e is the electronic charge. Therefore, flat band potential can be calculated by subtracting k_BT/e from the x-intercept in the linear plot of $1/C^2$ *vs.* V. The flat band potential is regarded as a potential of the valence band edge [30]. To examine accurate the band characteristics of CuO/Cu_2O

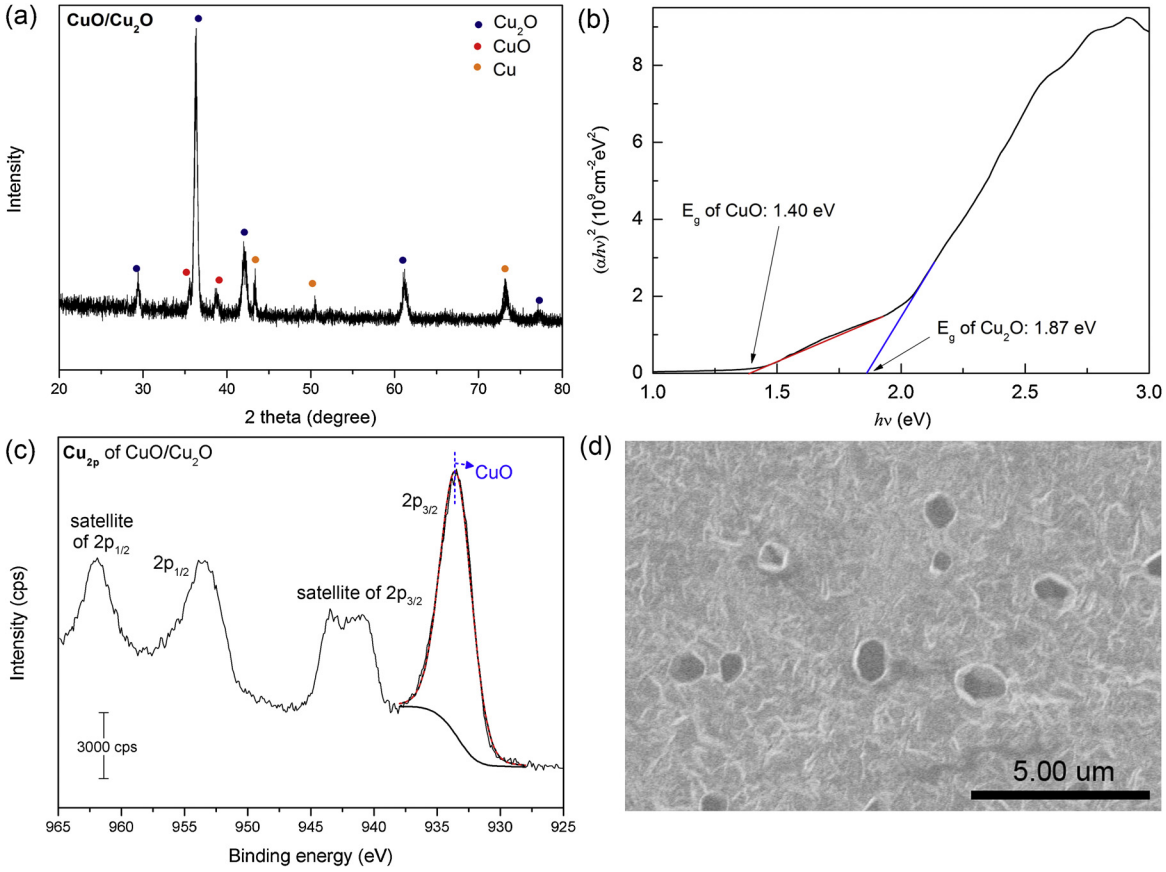

Fig. 1. (a) XRD result of CuO/Cu_2O thin film, (b) Band gap of CuO/Cu_2O calculated by UV–vis-NIR spectrometer measurement, (c) XPS data of CuO/Cu_2O, and (d) Top–down FESEM image of Pb metal deposited CuO/Cu_2O (representative image).

electrode in our case, Mott–Schottky plots at frequencies of 5 kHz and 10 kHz were collected from CuO and Cu_2O electrodes in 0.1 M $KHCO_3$ aqueous solution, respectively (Fig. S2(a) and (b)). The flat band potentials of CuO and Cu_2O were 0.67 V and 0.40 V (*vs.* SHE), respectively. The conduction band edges could be obtained by subtracting the measured band gaps (1.40 eV of CuO and 1.87 eV of Cu_2O by UV–vis-NIR spectrometer as shown in Fig. 1(b)) from the valence band edges (Fig. S2(c)).

3. Results and discussion

3.1. Characteristics of the CuO/Cu_2O

The layered structure of CuO/Cu_2O was confirmed by XRD, UV–vis-NIR spectrometer, and XPS analyses. In the XRD results (Fig. 1(a)), CuO and Cu_2O peaks emerged after oxidation of the Cu foil, indicating mixed phases of CuO and Cu_2O in the film. The UV–vis-NIR spectrometer also supported the presence of two different band gaps, observed at 1.40 eV and 1.87 eV (Fig. 1(b)) assigned to CuO and Cu_2O, respectively [25]. However, in the XPS analysis (Fig. 1(c)), which is a surface sensitive technique, only a CuO peak at 933 eV appeared in XPS-Cu_{2p}. This implied that CuO is the dominant surface product on the outer layer and Cu_2O is dominant in the inner layer of the prepared film. The distinctive layered structure was probably attributed to complete oxidation at the surface and partial oxidation of the inner film due to inadequate oxygen diffusion into the film. Deposition of transition metals on the CuO/Cu_2O electrodes, which was performed by photo-assisted electrodeposition, was confirmed by FESEM and EDS analyses. Fig. 1(d) shows a representative FESEM image among the metal deposited CuO/Cu_2O electrodes, Pb/CuO/Cu_2O. Regardless of the type of transition metals, the prepared films have similar morphologies and sizes of the surface-deposited metal particles, ranging from several hundred nanometers to several micrometers (Fig. S3). Moreover, similar amount of the metals (*i.e.* 0.31 ± 0.08 μmol/cm^2) were deposited on CuO/Cu_2O electrodes except for Ag (Table S1).

3.2. Photoelectrochemical activity of the Me/CuO/Cu_2Os

The CO_2 reduction in the photoelectrochemical system was examined by linear sweep voltammetry (LSV) and chronoamperometry in N_2- or CO_2-bubbled 0.1 M $KHCO_3$ aqueous solutions (pH 6.6–6.7) under irradiation of chopped visible light (a 450 W Xe lamp with a UV cut off filter, 400 nm < λ < 800 nm). Fig. 2 shows the photoelectrochemical responses of the bare CuO/Cu_2O. The results reveal higher reduction photocurrent under CO_2-bubbling than under a N_2-bubbling environment, indicating the CO_2 reducibility of bare CuO/Cu_2O. It has been reported that photocurrent in the N_2-bubbled electrolyte results from H_2 evolution or the innate properties of photocathode materials [10,25], and this would be further discussed in Section 3.3.

Interestingly, the Me/CuO/Cu_2O demonstrated improved photoelectrochemical activities of CO_2 reduction with higher onset potentials (Fig. S4). In the case of a p-type semiconductor in an electrolyte, there is an energy barrier between the semiconductor and the liquid electrolyte interface, and metal deposition on the semiconductor reduces energy loss in the interfacial reaction by decreasing the energy barrier of the junctions [12]. Therefore, deposited metals can facilitate electron transfer from the semiconductor to the liquid solution with reduced energy loss as well as acting as active sites [27,28]. The selectivity of fuel from CO_2

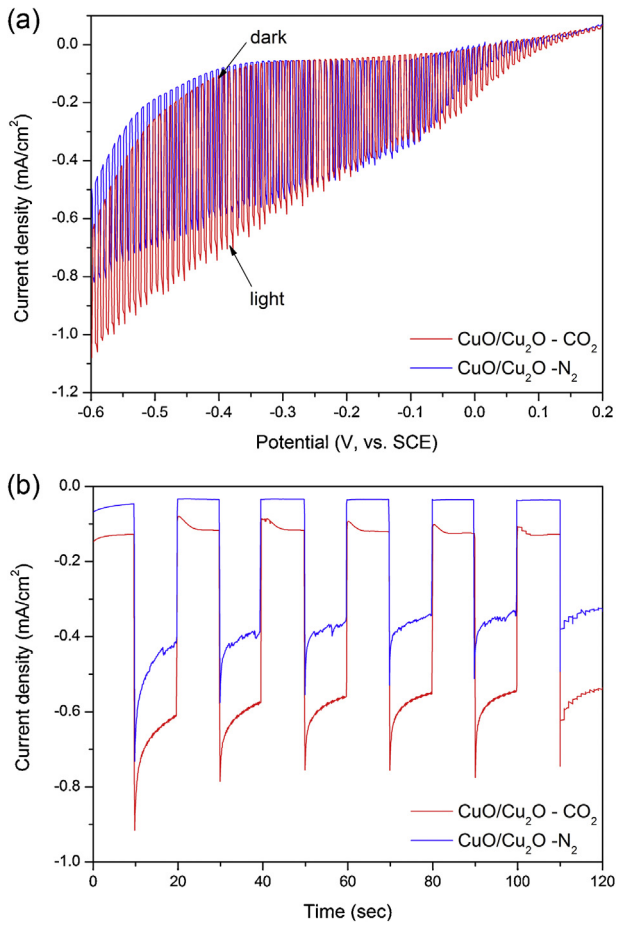

Fig. 2. CO_2 photoreduction activity of bare CuO/Cu_2O photocathode in N_2- and CO_2-gas bubbled 0.1 M $KHCO_3$ aqueous solution (pH 6.6–6.7) under irradiation of chopped visible light (a 450 W Xe lamp with UV cut off filter, $400 < \lambda < 800$) by LSV (a), and chronoamperometry at −0.4 V (*vs.* SCE) (b).

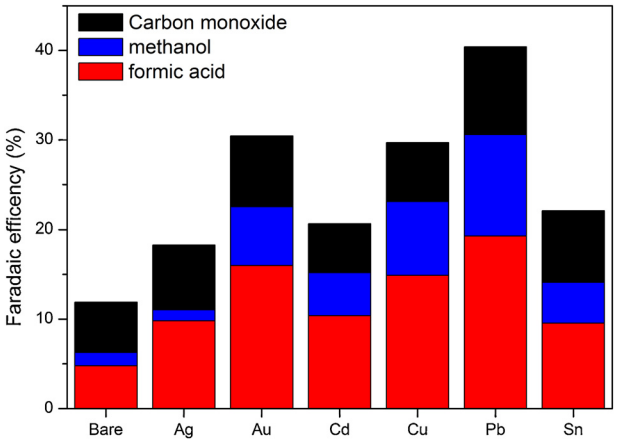

Fig. 3. Faradaic efficiencies of bare and metal-deposited CuO/Cu_2O photocathodes.

reduction was also determined according to the type of deposited transition metal [12,29].

A product analysis was performed in CO_2-bubbled 0.1 M $KHCO_3$ aqueous solutions under visible light irradiation for 1 h at −0.4 V (*vs.* SCE). It is worth noting that this potential is converted to −0.16 V (*vs.* SHE), which is much higher than the standard redox potential of formic acid (*ca.* −0.61 V *vs.* SHE), methanol (*ca.* −0.38 V *vs.* SHE), and carbon monoxide (*ca.* −0.53 V *vs.* SHE) formation from CO_2 [31]. However, the reduction of CO_2 at a more positive potential than the standard redox potentials was successfully performed due to the generation of photoenergy onto the CuO/Cu_2O film under the irradiation of visible light [30]. As shown in Table 1, bare CuO/Cu_2O shows 0.231 μmol/h cm^2 of formic acid and 0.024 μmol/h cm^2 of methanol in the photoelectrochemical CO_2 reduction. Otherwise, in the case of the $Me/CuO/Cu_2O$, metal-decorated film, improved activities for liquid fuel generations, from 0.329 to 0.602 μmol/h cm^2 for formic acid and from 0.054 to 0.110 μmol/h cm^2 for methanol, respectively, were observed. In particular, Cu and Pb demonstrated outstanding performances for liquid fuel generations among the transition metals: 0.602 μmol/h cm^2 of formic acid and 0.110 μmol/h cm^2 of methanol for Cu and 0.524 μmol/h cm^2 of formic acid and 0.102 μmol/h cm^2 of methanol for Pb. In electrochemical systems, research based on various transition metals has yielded similar results [3], indicating that the selectivity of CO_2 conversion products is determined by the type of metals, and Cu and Pb are promising electrocatalysts for liquid fuel generation. As gas products, CO dominantly evolved close to 0.258 ± 0.014 μmol/h cm^2, regardless of the type of metal, but H_2 was scarcely detected (Table 1). The absolute amounts of the products from the prepared photocathodes are comparable with previous studies: p-InP or p-CZTS with a Ru complex demanding a complicated fabrication process (Table S2) [9,15]. In terms of faradaic efficiency, the transition metal deposition on CuO/Cu_2O showed positive effects: 11.91% for bare CuO/Cu_2O but a dramatic increase to 18.29–40.45% for $Me/CuO/Cu_2Os$ (Fig. 3). However, the faradaic efficiency in this study is still lower than the values reported by other groups [7–9,11,15,16,25].

3.3. Investigation of photoelectrode degradation

The low faradaic efficiencies of $Me/CuO/Cu_2O$ electrodes resulted from the poor stabilities of the $Me/CuO/Cu_2O$ photocathode. Fig. 4(a) shows the performance profile of bare CuO/Cu_2O during 1 h of CO_2 reduction reaction. The performance rapidly decreased to ~30% after 20 min. In Fig. 4(b), the response from the chopped visible light irradiation also revealed fast degradation of photocurrent during the first 20 min.

This significant photocurrent disappearance was due to reduction of the surface CuO, which was confirmed by the XPS results of the photocathodes before and after the reaction (Fig. 5(a)). As shown in Fig. 5(a), the intensity of the CuO peak in XPS-Cu_{2p} decreased and the Cu_2O/Cu peak newly emerged after the reaction. This indicates that reduction from CuO to Cu_2O/Cu on the surface of the photocathode occurred during the reaction. This phenomenon was also observed in all of the $Me/CuO/Cu_2O$ photocathodes (Fig. 5(b) and Figs. S6–S8). The Pourbaix diagram also supports the results that Cu is the most stable phase under our experimental conditions with the pH and the applied potential we implemented (pH 6.6–6.7 and -0.16 V *vs.* SHE).

As shown in Table 1 and Fig. 3, the total faradaic efficiencies of the prepared electrodes for the CO_2 reductions were 11.91–40.45% for 1 h. However, the hydrogen gas was not detected in the reactions unlike many previous reports, and thus, the usage of residual currents is unclear. Hence, it was supposed that the residual currents were used for reducing CuO to Cu_2O/Cu, as shown in Fig. 5, and then the thickness of the reduce layer was mathematically calculated. This suggestion was fairly reasonable because CuO reduction ($E^0_{CuO/Cu}$ = 0.57 V *vs.* SHE at pH = 0) was thermodynamically more favorable than hydrogen evolution reaction (E^0_{H+/H_2} = 0 V *vs.* SHE at pH = 0), possibly resulting in dominant CuO reduction to Cu_2O/Cu rather than hydrogen evolution as demonstrated in XPS analysis (Fig. 5). We assumed that the outer layer of CuO was reduced to Cu having fcc crystal structure (Table S3). The predicted

Table 1
The results of photoelectrochemical CO_2 reduction in CO_2-bubbled 0.1 M $KHCO_3$ aqueous solution with prepared photocathodes (bare CuO/Cu_2O and $Me/CuO/Cu_2O$:Me=Ag, Au, Cd, Cu, Pb, and Sn) at −0.4 V (*vs.* SCE) under visible light irradiation.

	Charge[a] (C)	Formic acid (μmol/h cm^2)	F.E. (%)	Methanol (μmol/h cm^2)	F.E. (%)	CO (μmol/h cm^2)	F.E. (%)
Bare	0.93	0.231	4.78	0.024	1.49	0.250	5.64
Ag	0.72	0.368	9.81	0.015	1.23	0.272	7.25
Au	0.68	0.568	16.05	0.077	6.54	0.258	7.90
Cd	0.94	0.506	10.38	0.078	4.79	0.243	5.45
Cu	0.78	0.602	14.90	0.110	8.20	0.244	6.60
Pb	0.52	0.524	19.32	0.102	11.33	0.243	9.80
Sn	0.66	0.329	9.55	0.054	4.57	0.251	7.95

[a] Total charge used in CO_2 reduction reaction (= $\int I\,dt$; where I is the measured current and t is the reaction time) for 1 h in CO_2-bubbled 0.1 M $KHCO_3$ aqueous solution at −0.4 V (*vs.* SCE).

thicknesses of the Cu on the surface of the prepared electrodes were in the range of 114–302 nm. Considering the thickness of photoelectrochemical electrodes are generally reported with a few μm for efficient light utility [32,33], the calculated thickness is quite reasonable, corresponding to our assumption and inferring that the rest currents were consumed by the partial surface reduction of the CuO electrode.

However, a certain percentage of Cu_2O/Cu existed on the surface of $Me/CuO/Cu_2O$ electrodes before the reaction, which was caused by the partial surface reduction of $Me/CuO/Cu_2O$ electrodes for the photo-assisted electrodeposition step of metals, even if it took only 5 s. Nonetheless, the $Me/CuO/Cu_2O$ electrodes demonstrated increased faradaic efficiencies and selectivities for the CO_2 reduction reaction compared to those of the CuO/Cu_2O electrode. The reduced film-thicknesses for the metal deposition steps were very thin (less than 1 nm, Table S3), and thus, it can be concluded that the slight destruction of the less than 1 nm scarcely decreased the reaction kinetics.

The roles of metals as well as the effects of surface reduction were experimentally investigated by EIS studies of the CuO/Cu_2O and the $Au/CuO/Cu_2O$ electrodes (Fig. 6). Even though the semicircles in the EIS results are attributed to the combinations of the various reaction parameters (*e.g.* activation energy, kinetics, diffusion, resistance, etc.), it was very useful to study the effects of visible-light irradiation and the roles of metals. Fig. 6(a) showed that the diameter of a semicircle of CuO/Cu_2O decreases from 81 Ω to 76 Ω due to visible light irradiation, inferring the formation of photoexcited electrons having high energy. The

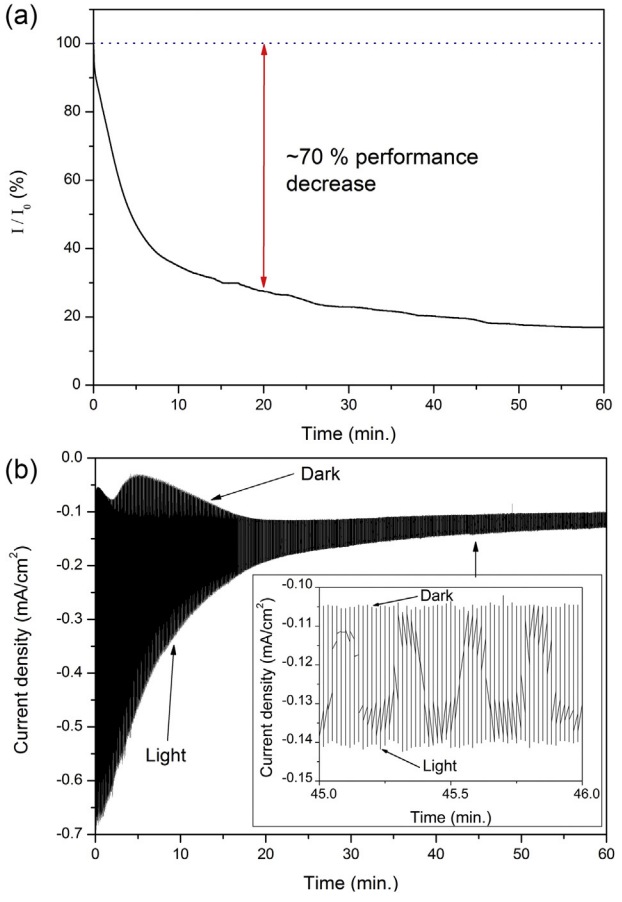

Fig. 4. (a) Performance degradation of CuO/Cu_2O during photoelectrochemical CO_2 reduction at −0.4 V (*vs.* SCE) for 1 h under visible light irradiation. (b) Photocurrent profile of CuO/Cu_2O at −0.4 V (*vs.* SCE) under chopped visible light irradiation (inset: focused graph on the range of 45–46 min).

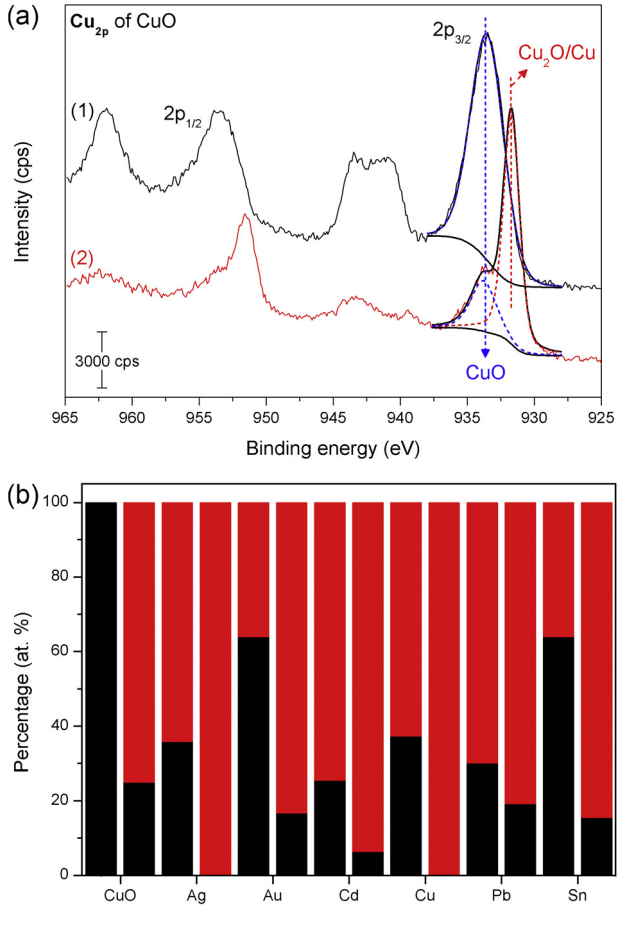

Fig. 5. (a) XPS data of bare CuO/Cu_2O before (black) and after reaction (red) (b) XPS–Cu_{2p} peak of CuO (black) and Cu_2O/Cu (red) of bare and metal decorated photocathodes ($Me/CuO/Cu_2O$) before (left bar) and after (right bar) reaction. (For interpretation of the references to color in this figure legend, the reader is referred to the web version of this article.)

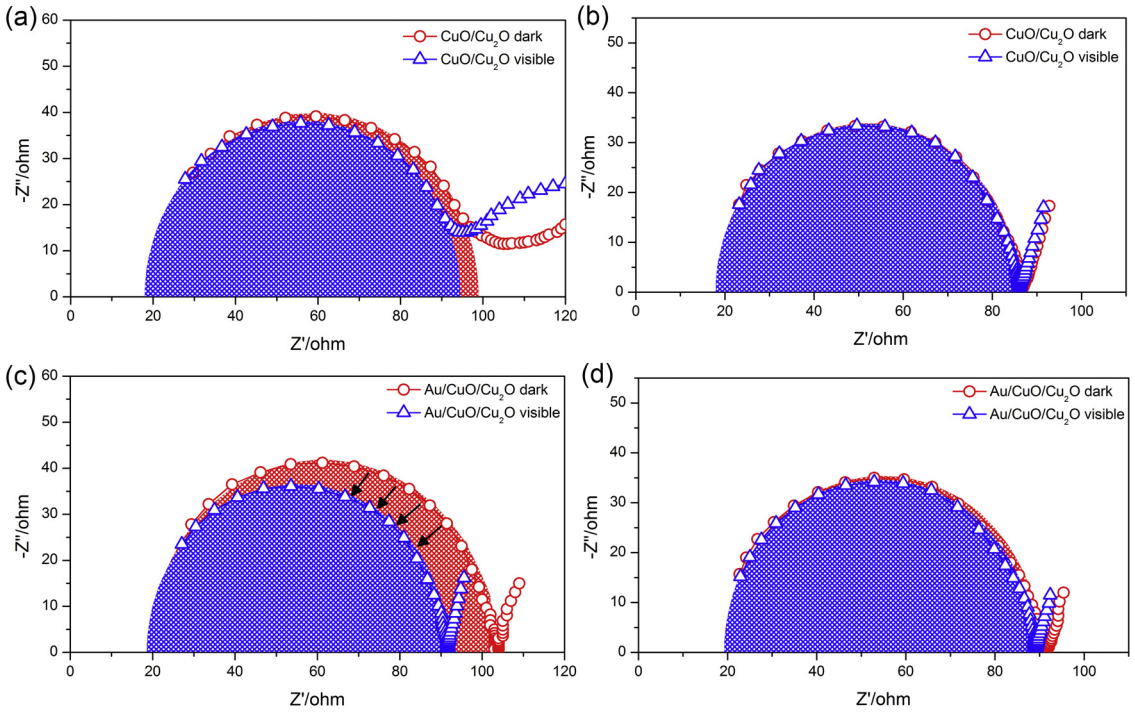

Fig. 6. Electrochemical impedance spectroscopy (EIS) measurements in CO_2-bubbled 0.1 M $KHCO_3$ at −0.4 V (*vs.* SCE) under dark (red) and visible light irradiation (blue) for CuO/Cu_2O photocathode (a) before and (b) after reaction, and those of $Au/CuO/Cu_2O$ photocathode (c) before and (d) after reaction. (For interpretation of the references to color in this figure legend, the reader is referred to the web version of this article.)

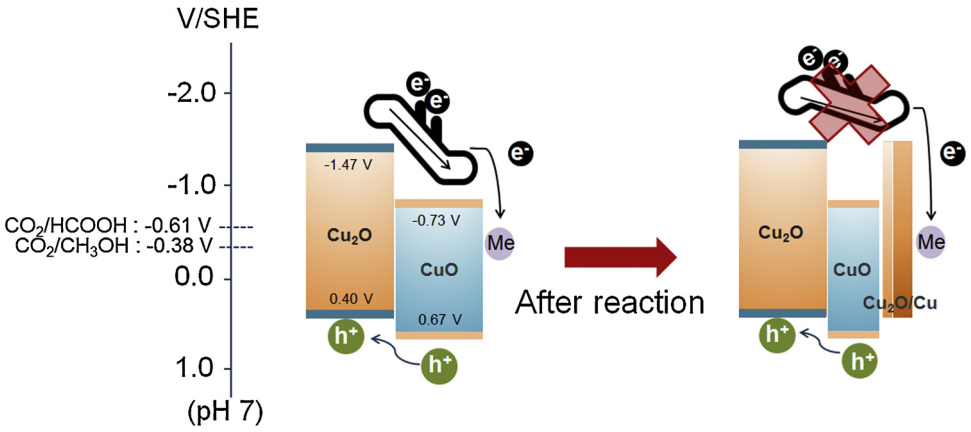

Fig. 7. Band structure of CuO/Cu_2O before (left) and after (right) reaction.

resistance value is greatly diminished from 84 Ω to 72 Ω for the $Au/CuO/Cu_2O$ electrode (Fig. 6(c)) with a difference of 12 Ω even though that of the bare CuO/Cu_2O electrode is only 5 Ω It implies that deposition of transition metals onto CuO/Cu_2O electrode improves the efficient electron transfer from semiconductor to electrolyte by suppressing the recombination of the photo generated carrier, which readily occurred in the case of bare CuO/Cu_2O electrode. In Fig. 6(b) and (d), both of bare CuO/Cu_2O and $Au/CuO/Cu_2O$ photocathodes show similar circle diameters regardless of light irradiation after the reaction, indicating the disappearance of the photo effects.

Based on the results, the proposed mechanism was described as a band diagram in Fig. 7. In the original structure of CuO/Cu_2O, photoexcited electrons are transferred from the conduction band of Cu_2O and CuO to the metal and finally are used in the CO_2 reduction reaction due to the different band positions of CuO and Cu_2O. At the same time, the holes flow along the valence band to the anode. Therefore, this electrode engineering is expected to generate effective electron–hole separation under photoenergy irradiation and provide a highway for facile electron migration to the active sites for CO_2 reduction. However, after the reaction, Cu_2O/Cu reduced from CuO on the surface destroys the electron–hole pathways, disturbing the efficient transfer of the charge carriers.

4. Conclusions

In this research, various transition metal-(*i.e.* Ag, Au, Cd, Cu, Pb and Sn)-decorated CuO/Cu_2O electrodes were designed as a promising strategy for efficient photoelectrochemical CO_2 reduction. Due to the different band positions of CuO and Cu_2O, the desirable electron–hole pathway from Cu_2O and CuO to active metals was provided in the layered structure of CuO/Cu_2O. Moreover, the metal deposition onto the surface of CuO/Cu_2O

were examined for reducing the energy loss in interfacial reactions as well as for controlling the selectivity of the products in terms of faradaic efficiency. Among the transition metals, Pb/CuO/Cu_2O exhibited the prominent CO_2 reduction reaction ability with 40.45% faradaic efficiency at −0.16 V (*vs.* SHE), which was much higher than the standard redox potential of the products. Furthermore, to investigate the origin of the performance degradation of prepared CuO/Cu_2O electrode during the reaction, XPS and EIS studies were conducted before and after the reaction. As a result, reduction of the outer layer CuO to Cu_2O/Cu was identified, and it caused interrupted flow of photogenerated carriers, inducing the disappearance of photocurrent. Moreover, EIS studies also implied that the metal deposition enhanced the efficient electron transfer to the active site with compressed electron–hole recombination.

Acknowledgments

The NMR experiments for liquid products analysis were performed on Bruker Avance 800 MHz spectrometer at the Korea Basic Science Institute (KBSI). This research is supported by BK21PLUS program (Sustainable Energy Science and Engineering) through the National Research Foundation (NRF), Republic of Korea.

Appendix A. Supplementary data

Supplementary data associated with this article can be found, in the online version, at http://dx.doi.org/10.1016/j.apcatb.2014.04.021.

References

[1] A. Andrea, N.C. Eric, A.R. Mark, L. Stephanie, R.E. Lindsey, E.M. James, B.S. Ellen, Synthesis and characterization of ferrite materials for thermochemical CO_2 splitting using concentrated solar energy, in: Advances in CO_2 Conversion and Utilization, American Chemical Society, New Mexico, 2010, pp. 1–13.
[2] B. Lu, K. Kawamoto, J. Environ. Chem. Eng. 1 (2013) 300–309.
[3] M. Azuma, K. Hashimoto, M. Hiramoto, M. Watanabe, T. Sakata, J. Electrochem. Soc. 137 (1990) 1772–1778.
[4] M. Gattrell, N. Gupta, A. Co, J. Electroanal. Chem. 594 (2006) 1–19.
[5] E.E. Barton, D.M. Rampulla, A.B. Bocarsly, J. Am. Chem. Soc. 130 (2008) 6342–6344.
[6] M. Halmann, Nature 275 (1978) 115–116.
[7] T. Arai, S. Sato, T. Kajino, T. Morikawa, Energy Environ. Sci. 6 (2013) 1274–1282.
[8] S. Sato, T. Arai, T. Morikawa, K. Uemura, T.M. Suzuki, H. Tanaka, T. Kajino, J. Am. Chem. Soc. 133 (2011) 15240–15243.
[9] T. Arai, S. Sato, K. Uemura, T. Morikawa, T. Kajino, T. Motohiro, Chem. Commun. 46 (2010) 6944–6946.
[10] T.J. LaTempa, S. Rani, N.Z. Bao, C.A. Grimes, Nanoscale 4 (2012) 2245–2250.
[11] B. Kumar, J.M. Smieja, C.P. Kubiak, J. Phys. Chem. C 114 (2010) 14220–14223.
[12] R. Hinogami, Y. Nakamura, S. Yae, Y. Nakato, J. Phys. Chem. B 102 (1998) 974–980.
[13] H. Yoneyama, K. Sugimura, S. Kuwabata, J. Electroanal. Chem. 249 (1988) 143–153.
[14] J.H. Jeon, P.M. Mareeswaran, C.H. Choi, S.I. Woo, RSC Adv. 4 (2014) 3016–3019.
[15] T. Arai, S. Tajima, S. Sato, K. Uemura, T. Morikawa, T. Kajino, Chem. Commun. 47 (2011) 12664–12666.
[16] J.L. Yuan, C.J. Hao, Sol. Energy Mater. Sol. Cells 108 (2013) 170–174.
[17] A.B. Bocarsly, Q.D. Gibson, A.J. Morris, R.P. L'Esperance, Z.M. Detweiler, P.S. Lakkaraju, E.L. Zeitler, T.W. Shaw, ACS Catal. 2 (2012) 1684–1692.
[18] J.H. Montoya, A.A. Peterson, J.K. Norskov, ChemCatChem 5 (2013) 737–742.
[19] Z.F. Chen, P. Kang, M.T. Zhang, B.R. Stoner, T.J. Meyer, Energy Environ. Sci. 6 (2013) 813–817.
[20] C.W. Li, M.W. Kanan, J. Am. Chem. Soc. 134 (2012) 7231–7234.
[21] K.P. Kuhl, E.R. Cave, D.N. Abram, T.F. Jaramillo, Energy Environ. Sci. 5 (2012) 7050–7059.
[22] M. Le, M. Ren, Z. Zhang, P.T. Sprunger, R.L. Kurtz, J.C. Flake, J. Electrochem. Soc. 158 (2011) E45–E49.
[23] S. Ohya, S. Kaneco, H. Katsumata, T. Suzuki, K. Ohta, Catal. Today 148 (2009) 329–334.
[24] P. Li, H. Wang, J. Xu, H. Jing, J. Zhang, H. Han, F. Lu, Nanoscale 5 (2013) 11748–11754.
[25] G. Ghadimkhani, N.R. de Tacconi, W. Chanmanee, C. Janaky, K. Rajeshwar, Chem. Commun. 49 (2013) 1297–1299.
[26] K. Rajeshwar, N.R. de Tacconi, G. Ghadimkhani, W. Chanmanee, C. Janáky, ChemPhysChem 14 (2013) 2251–2259.
[27] X. Feng, J.D. Sloppy, T.J. LaTempa, M. Paulose, S. Komarneni, N. Bao, C.A. Grimes, J. Mater. Chem. 21 (2011) 13429–13433.
[28] O.K. Varghese, M. Paulose, T.J. LaTempa, C.A. Grimes, Nano Lett. 9 (2009) 731–737.
[29] X. Li, Z. Zhuang, W. Li, H. Pan, Appl. Catal., A: Gen. 429–430 (2012) 31–38.
[30] J. Gu, A. Wuttig, J.W. Krizan, Y. Hu, Z.M. Detweiler, R.J. Cava, A.B. Bocarsly, J. Phys. Chem. C 117 (2013) 12415–12422.
[31] B. Kumar, M. Llorente, J. Froehlich, T. Dang, A. Sathrum, C.P. Kubiak, Annu. Rev. Phys. Chem. 63 (2012) 541–569.
[32] A. Hagfeldt, U. Björkstén, S.-E. Lindquist, Sol. Energy Mater. Sol. Cells 27 (1992) 293–304.
[33] S. Soedergren, A. Hagfeldt, J. Olsson, S.-E. Lindquist, J. Phys. Chem. 98 (1994) 5552–5556.